

Monte Carlo simulation of runaway MeV electron breakdown with application to red sprites and terrestrial gamma ray flashes

N. G. Lehtinen, T. F. Bell, and U. S. Inan
STAR Laboratory, Stanford University, Stanford, California

Abstract

A three-dimensional Monte Carlo model of the uniform relativistic runaway electron breakdown in air in the presence of static electric and magnetic fields is used to calculate electron distribution functions, avalanche rates, and the direction and velocity of avalanche propagation. We also derive the conditions required for an electron with a given momentum to start an avalanche in the absence of a magnetic field. The results are compared to previously developed kinetic and analytical models and our own analytical estimates, and it is concluded that the rates used in many early models [e.g., *Lehtinen et al.*, 1997; *Taranenko and Roussel-Dupré*, 1996; *Yukhimuk et al.*, 1998; *Roussel-Dupré et al.*, 1998] are overestimated by a factor of ~ 10 . The Monte Carlo simulation results are applied to a fluid model of runaway electron beams in the middle atmosphere accelerated by quasi-electrostatic fields following a positive lightning stroke. In particular, we consider the case of lightning discharges which drain positive charge from remote regions of a laterally extensive (> 100 km) thundercloud, using a Cartesian two-dimensional model. The resulting optical emission intensities in red sprites associated with the runaway electrons are found to be negligible compared to the emissions from thermal electrons heated in the conventional type of breakdown. The calculated gamma ray flux is of the same order as the terrestrial gamma ray flashes observed by the Burst and Transient Source Experiment detector on the Compton Gamma Ray Observatory.

1. Introduction

Red sprites [Sentman *et al.*, 1995] are large-scale luminous glows occurring above thunderstorms at altitudes 50–90 km, exhibiting predominantly red color. Terrestrial gamma ray flashes have been observed by the Burst and Transient Source Experiment (BATSE) detectors located on the Compton Gamma Ray Observatory (CGRO) [Fishman *et al.*, 1994] and are believed to be associated with lightning discharges [Inan *et al.*, 1996]. In this work, we apply a new Monte Carlo model to evaluate the connection of the red sprites and terrestrial gamma ray flashes with high-energy (20 keV to 10 MeV) runaway electrons, produced above thunderstorms and driven upward by the thundercloud electric field.

1.1. Runaway Breakdown in Gases

When the energy of an electron in a gas exceeds a certain value, the friction force resulting from its collisions with the gas constituents begins to decrease with increasing energy, as shown by the solid line in Figure 1. If a strong enough external electric force is applied to such an electron, it becomes a “runaway” electron and initiates a breakdown process.

The runaway electron breakdown was previously studied not only in relation to non-ionized air but also in relation to high-energy plasmas, such as in tokamaks and astrophysical plasmas. Analytical studies considered uniform breakdown [Sizykh, 1993; Gurevich *et al.*, 1992], spatial propagation and diffusion of a runaway beam [Gurevich *et al.*, 1994], breakdown in the presence of a magnetic field [Gurevich *et al.*, 1996], and the runaway process in a high-energy plasma [Bulanov *et al.*, 1997]. The numerical solution of the kinetic equation describing the relativistic runaway breakdown in the absence of a magnetic field was obtained in air [Roussel-Dupré *et al.*, 1994; Symbalisty *et al.*, 1998] and in high-energy helium [Babich and Kutsyk, 1995]. One-dimensional (1-D) Monte Carlo models of thermal runaway with strong fields $E/N > 3 \times 10^{-19} \text{ V m}^2$ were applied to nitrogen [Kurnhardt *et al.*, 1986] and neon [Shveigert, 1988].

In an earlier study of runaway electrons [Lehtinen *et al.*, 1997], the avalanche rates were taken from a nonmagnetic kinetic model [Roussel-Dupré *et al.*, 1994], and the direction of avalanche propagation was calculated from the equation of motion of an individual electron [Gurevich *et al.*, 1996].

It has since been shown [Symbalisty *et al.*, 1997]

that the avalanche rates as reported by Roussel-Dupré *et al.* [1994] were not accurate, both because of numerical problems in the computations and owing to the fact that the effects of the magnetic field were neglected.

In this paper we use a Monte Carlo technique in order to model runaway avalanche in the presence of a magnetic field. This more general method also allows us to address existing discrepancies between the results of different models of this phenomenon. Avalanche rates and the direction and velocity of avalanche propagation are accurately determined from our Monte Carlo model and then used in the 2-D Cartesian runaway model in the middle atmosphere.

1.2. Runaway Breakdown in the Middle Atmosphere

The relativistic runaway breakdown field E_t in air above thunderclouds [Gurevich *et al.*, 1992] is smaller than the conventional breakdown field [Papadopoulos *et al.*, 1993] by a factor of ~ 10 . The runaway electrons are thought to be accelerated by quasi-electrostatic fields in the middle atmosphere following a positive cloud-to-ground (+CG) discharge [Bell *et al.*, 1995]. The seed of the relativistic runaway electron avalanche is provided by MeV electrons from a cosmic ray shower [McCarthy and Parks, 1992].

In our previous work [Lehtinen *et al.*, 1997], we studied the production of runaway electrons in thunderstorms using a cylindrically symmetric model with vertical axis and vertical geomagnetic field. Red sprites have been observed at magnetic latitudes ranging from 10° to 50° , and terrestrial gamma ray flashes have been observed throughout the equatorial region covered by CGRO, namely $\pm 20^\circ$ geographic latitude. These low-latitude regions are characterized by a large angle between geomagnetic field and the vertical, which makes the cylindrically symmetric model inadequate to describe energetic electron discharges, since the magnetic field influences the electron motion to a large extent at high altitudes [Lehtinen *et al.*, 1997; Gurevich *et al.*, 1996].

The Monte Carlo model considered here allows an arbitrary direction of the geomagnetic field. The model is also two-dimensional but is translationally symmetric in a horizontal direction and is applicable to the case of lightning draining positive charge from remote regions of a laterally extensive ($> 100 \text{ km}$) storm front. The length of the cloud must be at least the size of the region modeled. The discharge

in our model is characterized by the removal of a linear charge density (in C/km).

We calculate both optical emission in the N₂ first positive band system, which is dominant in red sprites, and gamma ray emission from energetic runaways [Lehtinen *et al.*, 1996]. The gamma ray flux and spectrum are compared to BATSE observations [Nemiroff *et al.*, 1997].

2. Breakdown Simulation

In this work, we use the following notations:

- E, B** external electric and magnetic fields, assumed constant and uniform in the Monte Carlo calculations;
- p, \mathcal{E} , v** electron momentum, kinetic energy and velocity, respectively;
- $\gamma = 1/\sqrt{1-v^2/c^2} = 1 + \frac{\mathcal{E}}{mc^2}$ electron relativistic factor;
- N_m molecular density of air;
- $Z_m = 14.5$ average molecular nuclear charge for air;
- e magnitude of the electron charge;
- m electron mass;
- c speed of light;
- $r_0 = e^2/(4\pi\epsilon_0 mc^2) \approx 2.81777 \times 10^{-15}$ m electron classical radius.

2.1. General Description

The Monte Carlo model of runaway breakdown makes use of a set of test electrons, for which phase space coordinate information is stored. The motion of energetic electrons is described by the Langevin equation. It includes the electric and magnetic forces and a stochastic force $\mathbf{\Gamma}(t)$, which describes the elastic and inelastic scattering of electrons:

$$\frac{d\mathbf{p}}{dt} = -e\mathbf{E} - \frac{e}{m\gamma}\mathbf{p} \times \mathbf{B} + \mathbf{\Gamma}(t). \quad (1)$$

The model is based on solving equation (1) numerically for each electron in the set, with a time step Δt . The collision term $\mathbf{\Gamma}$ is divided into two parts, one described in terms of a dynamic friction function and the other determined on a statistical basis. The latter involves the nonzero probability that some of the collisions lead to the generation of new energetic electrons by ionization, which must be added to the existing set of test electrons.

Typically, there are many more electrons at lower energies than at higher energies due to the $(\mathcal{E}')^{-2}$ dependence of the ionization probability for creation of

an electron of energy \mathcal{E}' , as is shown later. For simplicity, we only consider electrons with $\mathcal{E} > \mathcal{E}_{\min}$ and choose $\mathcal{E}_{\min} = 2$ keV. Any electrons for which the kinetic energy decreases below \mathcal{E}_{\min} are dropped from the set. For an ionizing collision leading to the production of a secondary electron with energy $\mathcal{E}' > \mathcal{E}_{\min}$, momentum vectors of both electrons after the ionizing collision are calculated on the basis of the ionization cross section. For $\mathcal{E}' < \mathcal{E}_{\min}$, the processes of energy loss and velocity direction change are described in terms of the dynamic friction function and angular diffusion, respectively.

2.2. Dynamic Friction Function (Stopping Power)

The energy losses for energetic electron motion in a collisional gas are due to excitation and ionization processes and can be described in terms of a dynamic friction force $F_D(\mathcal{E})$ [Bethe and Ashkin, 1953, p. 254], effectively acting in the direction opposite to the electron motion:

$$F_D(\mathcal{E}) = N_m Z_m \kappa \left\{ \ln \frac{mv^2 \mathcal{E}}{I^2(1-v^2/c^2)} - \left(1 + \frac{2}{\gamma} - \frac{1}{\gamma^2} \right) \ln 2 + \frac{(\gamma-1)^2}{8\gamma^2} + \frac{1}{\gamma^2} \right\}, \quad (2)$$

where

$$\kappa = 2\pi r_0^2 mc^2 (c/v)^2 \quad (3)$$

and I is the average ionization energy, $I \approx 80.5$ eV for air [Roussel-Dupré *et al.*, 1994]. This force has a minimum at electron kinetic energy $\mathcal{E} \approx 2.39 \times mc^2 \approx 1.22$ MeV, which is equal to electric force due to the runaway threshold field E_t , determined by

$$\frac{E_t}{N_m} \approx 21.7 \times 2\pi Z_m r_0^2 mc^2 e^{-1} \approx 8.05 \times 10^{-21} \text{ V m}^2 = 8.05 \text{ Td}, \quad (4)$$

where Td is a townsend, a convenient unit of E/N .

Because the ionization with creation of electrons with energy $\mathcal{E}' > \mathcal{E}_{\min}$ is included explicitly in our model, we must exclude the energy losses associated with it from the dynamic friction:

$$F_{D,\text{excl}}(\mathcal{E}) = F_D(\mathcal{E}) - F_{D,\text{ion}}(\mathcal{E}). \quad (5)$$

The ionization loss is (we neglect the ionization energy $I \ll \mathcal{E}_{\min}$):

$$F_{D,\text{ion}}(\mathcal{E}) = N_m Z_m \int_{\mathcal{E}_{\min}}^{\mathcal{E}/2} \mathcal{E}' \frac{\partial \sigma_{\text{ion}}}{\partial \mathcal{E}'}(\mathcal{E}, \mathcal{E}') d\mathcal{E}', \quad (6)$$

The cross section for ionization σ_{ion} is given by Møller formula (see expression (14) below). Electrons emerging in a collision are indistinguishable, and we label the one with the lower energy as the secondary electron. Therefore the maximum energy that can be lost in a collision is $\mathcal{E}/2$.

After substituting the Møller cross section we find

$$F_{D,\text{ion}}(\mathcal{E}) = N_m Z_m \kappa \left\{ \ln \frac{\mathcal{E}}{2\mathcal{E}_{\min}} + \frac{(\gamma-1)^2}{8\gamma^2} - \frac{\mathcal{E}_{\min}^2}{2(mc^2 + \mathcal{E})^2} - \left(1 + \frac{2}{\gamma} - \frac{1}{\gamma^2}\right) \ln \frac{2(\mathcal{E} - \mathcal{E}_{\min})}{\mathcal{E}} + 1 - \frac{\mathcal{E}_{\min}}{\mathcal{E} - \mathcal{E}_{\min}} \right\}, \quad (7)$$

$$F_{D,\text{excl}}(\mathcal{E}) = N_m Z_m \kappa \left\{ \ln \frac{2\mathcal{E}_{\min} m v^2}{I^2(1 - v^2/c^2)} - \left(1 + \frac{2}{\gamma} - \frac{1}{\gamma^2}\right) \ln \frac{\mathcal{E}}{\mathcal{E} - \mathcal{E}_{\min}} + \frac{\mathcal{E}_{\min}}{\mathcal{E} - \mathcal{E}_{\min}} - \frac{v^2}{c^2} + \frac{\mathcal{E}_{\min}^2}{2(mc^2 + \mathcal{E})^2} \right\}. \quad (8)$$

Note that equation (6) is meaningful only for $\mathcal{E} \geq 2\mathcal{E}_{\min}$, and therefore for $\mathcal{E}_{\min} < \mathcal{E} < 2\mathcal{E}_{\min}$ we still use expression (2) instead of equation (8). Both $F_D(\mathcal{E})$ and $F_{D,\text{excl}}(\mathcal{E})$ are plotted in Figure 1 as functions of \mathcal{E} .

For the electron energies of interest in the mesosphere (< 100 MeV, as limited by the electric potential difference between the thundercloud and the ionosphere), the radiative losses due to bremsstrahlung are negligible [Jackson, 1975, p. 718] and are not accounted for in our model.

2.3. Angular Diffusion

The angular scattering of electrons is mostly due to their elastic collisions with nuclei. The contribution of this process is by a factor of atomic charge $Z_a = Z_m/2$ greater than the contribution of collisions with electrons.

Although the elastic collisions are frequent, the average angle of scattering is small, and we can choose our time step Δt much greater than the time between collisions. We incorporate small-angle collisions into the Monte Carlo model as random changes of \mathbf{p} direction by an angle $\Delta\Theta$.

To find $\Delta\Theta$ for given Δt , we calculate a random variable $\mu = \cos(\Delta\Theta)$, which has a probability distribution $f(\mu, t = \Delta t)$. This distribution is normalized

to 1:

$$\int_{-1}^1 f(\mu, t) d\mu = 1$$

and satisfies initial condition such that $f \neq 0$ only at $\Delta\Theta = 0$ (the direction of an electron is fixed):

$$f(\mu, t = 0) = \delta(\mu - 1_-),$$

where by 1_- we mean that the delta function is fully included when integrated with upper limit 1. The probability distribution function $f(\mu, t)$ satisfies the diffusion equation [Roussel-Dupr e et al., 1994]:

$$\frac{\partial f}{\partial t} = D \frac{\partial}{\partial \mu} \left\{ (1 - \mu^2) \frac{\partial f}{\partial \mu} \right\}$$

The diffusion coefficient is connected with the time rate of change of the mean square angle:

$$D(p) = \frac{1}{4} \frac{d\langle\Theta^2\rangle}{dt},$$

an explicit expression for which is derived below. The solution to the diffusion equation is

$$f(\mu, \Delta t) = \sum_{n=0}^{\infty} \left(n + \frac{1}{2} \right) P_n(\mu) e^{-Dn(n+1)\Delta t}, \quad (9)$$

where P_n are Legendre polynomials. For $D\Delta t \gtrsim 1$ in calculations we take into account only the terms $n = 0$ and 1 in equation (9). For $D\Delta t \ll 1$, equation (9) can be approximated as

$$f(\mu, \Delta t) \approx \frac{1}{2D\Delta t} \exp\left(\frac{\mu-1}{2D\Delta t}\right). \quad (10)$$

For very small scattering angle $\Delta\Theta$, equation (10) is not well suited for computation because of a small number in the denominator. In such cases we take a fixed $\Delta\Theta$ [Risken, 1989, p. 60]:

$$\Delta\Theta \equiv \sqrt{\langle\Theta^2\rangle} = \sqrt{\frac{d\langle\Theta^2\rangle}{dt} \Delta t}. \quad (11)$$

Equation (11) is valid for multiple scattering for a distribution of the random single-scattering angle with a finite variance. This is true here because the singularity of Rutherford formula for the scattering cross section at small angles is absent due to screening which is discussed shortly.

The rate of time change of the mean square angle for electrons, scattered by neutral atoms is [Jackson, 1975, p. 649]:

$$\frac{d\langle\Theta^2\rangle}{dt} = v \frac{d\langle\Theta^2\rangle}{ds} = 2\pi N_a v \left(\frac{2Z_a r_0 c^2}{\gamma v^2} \right)^2 \ln \frac{\theta_{\max}}{\theta_{\min}}, \quad (12)$$

where $N_a = 2N_m$ is the number density of atoms. The angle θ_{\min} is the minimum angle of scattering, below which the scattered angular distribution falls substantially below the Rutherford formulas for a Coulomb potential. It is determined by Fermi-Thomas screening of the nucleus by bound electrons. The angle θ_{\max} for electrons is ~ 1 for electrons in air with energy less than ~ 50 MeV, so that the size of the nucleus is not important [Jackson, 1975, p. 646]. The minimum angle is $\theta_{\min} = Z_a^{1/3}(mc/p)/x$, where $x = 192$ [Jackson, 1975, p. 645], or $x = 65.3$ [Mott and Massey, p. 469]. In our code we choose (C. L. Longmire and H. J. Longley, unpublished report, 1973) $\theta_{\max} = 2$ and θ_{\min} from [Mott and Massey, 1965]. Upon substitution, we find

$$\frac{d\langle\Theta^2\rangle}{dt} = \frac{4\pi N_m Z_m^2 r_0^2 c^4}{v^3 \gamma^2} \log\left(\frac{164.7}{Z_m^{1/3}} \frac{p}{mc}\right). \quad (13)$$

2.4. Production of New Electrons

Production of secondary electrons in ionizing collisions is described by the Møller formula for relativistic scattering of two free electrons, one of them being initially at rest. In this way, we neglect the ionization energy $I \ll \mathcal{E}_{\min}$. The cross section into unit energy interval is

$$\begin{aligned} \frac{\partial\sigma_{\text{ion}}}{\partial\mathcal{E}'}(\mathcal{E}, \mathcal{E}') = & \kappa \left\{ \frac{1}{\mathcal{E}'^2} - \frac{1}{(\mathcal{E} - \mathcal{E}')\mathcal{E}'} \frac{(2\mathcal{E} + mc^2)mc^2}{(\mathcal{E} + mc^2)^2} + \frac{1}{(\mathcal{E} - \mathcal{E}')^2} \right. \\ & \left. + \frac{1}{(\mathcal{E} + mc^2)^2} \right\}, \quad (14) \end{aligned}$$

where κ is defined in equation (3), \mathcal{E} is the initial kinetic energy, and \mathcal{E}' is the kinetic energy of secondary electron after collision.

The total ionization cross section for the secondary electron energy $\mathcal{E}' > \mathcal{E}_{\min}$ is

$$\begin{aligned} \sigma_{\text{tot}}(\mathcal{E}) &= \int_{\mathcal{E}_{\min}}^{\mathcal{E}/2} \frac{\partial\sigma_{\text{ion}}}{\partial\mathcal{E}'}(\mathcal{E}, \mathcal{E}') d\mathcal{E}' \\ &= \kappa \left\{ \frac{1}{\mathcal{E}_{\min}} - \frac{1}{\mathcal{E} - \mathcal{E}_{\min}} + \frac{\mathcal{E} - 2\mathcal{E}_{\min}}{2(mc^2 + \mathcal{E})^2} + \right. \\ & \quad \left. \frac{mc^2(mc^2 + 2\mathcal{E})}{\mathcal{E}(mc^2 + \mathcal{E})^2} \ln \frac{\mathcal{E}_{\min}}{\mathcal{E} - \mathcal{E}_{\min}} \right\}. \quad (15) \end{aligned}$$

The probability of ionization during time step Δt by an electron is then

$$P = N_m Z_m v \sigma_{\text{tot}}(\mathcal{E}) \Delta t. \quad (16)$$

The random secondary electron energy \mathcal{E}_{sec} in the code is found on the basis of the random variable

$$X(\mathcal{E}_{\text{sec}}) = \frac{1}{\sigma_{\text{tot}}(\mathcal{E})} \int_{\mathcal{E}_{\min}}^{\mathcal{E}_{\text{sec}}} \frac{\partial\sigma_{\text{ion}}}{\partial\mathcal{E}'}(\mathcal{E}, \mathcal{E}') d\mathcal{E}', \quad (17)$$

uniformly distributed in the interval $[0, 1]$. Inversion of (17) to find \mathcal{E}_{sec} is done using approximate expressions

$$\begin{aligned} \frac{\partial\sigma_{\text{ion}}}{\partial\mathcal{E}'}(\mathcal{E}, \mathcal{E}') &\approx \frac{\kappa}{\mathcal{E}'^2} \\ \int_{\mathcal{E}_{\min}}^{\mathcal{E}_{\text{sec}}} \frac{\partial\sigma_{\text{ion}}}{\partial\mathcal{E}'}(\mathcal{E}, \mathcal{E}') d\mathcal{E}' &\approx \kappa \left(\frac{1}{\mathcal{E}_{\min}} - \frac{1}{\mathcal{E}_{\text{sec}}} \right) \\ \sigma_{\text{tot}}(\mathcal{E}) &\approx \int_{\mathcal{E}_{\min}}^{\mathcal{E}/2} \frac{\kappa}{\mathcal{E}'^2} d\mathcal{E}' \\ &= \kappa \left(\frac{1}{\mathcal{E}_{\min}} - \frac{2}{\mathcal{E}} \right), \end{aligned}$$

so that

$$\mathcal{E}_{\text{sec}} \approx \frac{\mathcal{E}\mathcal{E}_{\min}}{\mathcal{E} - X(\mathcal{E} - 2\mathcal{E}_{\min})}. \quad (18)$$

Numerical inversion of $X(\mathcal{E}_{\text{sec}})$ using the exact expression (17) can be done using Newton's method, but does not give significantly increased precision compared to using equation (18). In fact, the error in \mathcal{E}_{sec} as determined with equation (18) does not exceed $\sim 5\%$.

The components of the electron momenta after the collision are determined from the conservation of energy and momentum. The angles are most efficiently found from scalar products of energy-momentum four vectors of electrons before and after a collision. For example, if \mathbf{p}_0 , \mathbf{p}_{rest} , and \mathbf{p}_1 , \mathbf{p}_2 are respectively the energy-momentum four vectors of the moving and resting electrons before and after a collision, then $\mathbf{p}_0 = \{mc\gamma_0, \mathbf{p}_0\}$, $\mathbf{p}_{\text{rest}} = \{mc, \mathbf{0}\}$, $\mathbf{p}_1 = \{mc\gamma_1, \mathbf{p}_1\}$, $\mathbf{p}_2 = \{mc\gamma_2, \mathbf{p}_2\}$, and $\mathbf{p}_{\text{rest}} + \mathbf{p}_0 = \mathbf{p}_1 + \mathbf{p}_2$. Using the fact that $\mathbf{p}^2 = \mathbf{p} \cdot \mathbf{p} \equiv m^2 c^2 \gamma^2 - |\mathbf{p}|^2 = m^2 c^2$ for any electron state, from $(\mathbf{p}_0 - \mathbf{p}_1)^2 = (\mathbf{p}_2 - \mathbf{p}_{\text{rest}})^2$ we promptly find $\mathbf{p}_0 \cdot \mathbf{p}_1 = m^2 c^2 (\gamma_0 \gamma_1 - \gamma_2)$ and

$$\cos(\widehat{\mathbf{p}_0, \mathbf{p}_1}) = \sqrt{\frac{\mathcal{E}_1(\mathcal{E}_0 + 2mc^2)}{\mathcal{E}_0(\mathcal{E}_1 + 2mc^2)}}, \quad (19a)$$

$$\sin(\widehat{\mathbf{p}_0, \mathbf{p}_1}) = \sqrt{\frac{mc^2(\mathcal{E}_0 - \mathcal{E}_1)}{\mathcal{E}_0(\mathcal{E}_1 + 2mc^2)}}, \quad (19b)$$

where $\mathcal{E}_i = mc^2(\gamma_i - 1)$ are kinetic energies of corresponding electrons and where we have used $|\mathbf{p}| = mc\sqrt{\gamma^2 - 1}$ for each state and $\gamma_2 = \gamma_0 + 1 - \gamma_1$. The

direction of the momentum of the other electron is found by substituting indices $1 \rightarrow 2$. The angles for electron directions were also given in previous works on runaway [e.g., Roussel-Dupré et al., 1994].

2.5. Dimensionless Variables

To simplify numerical coefficients in the equations describing collisional processes in the program, we use dimensionless values of electron momentum, energy and velocity, and time:

$$\mathcal{E}_d = \frac{\mathcal{E}}{mc^2}, \quad \mathbf{p}_d = \frac{\mathbf{p}}{mc}, \quad \mathbf{v}_d \equiv \beta = \frac{\mathbf{v}}{c}, \quad t_d = \frac{t}{\tau}, \quad (20)$$

where

$$\tau = (2\pi N_m Z_m r_0^2 c)^{-1} \quad (21)$$

is a characteristic time of the process. With this choice, $N_m Z_m \kappa / (mc\tau) = \beta^{-2}$ and the equation of motion (1) does not depend on N_m and therefore on the altitude at which the process occurs. The sea level value of $N_m \approx 2.688 \times 10^{25} \text{ m}^{-3}$ corresponds to $\tau \approx 172 \text{ ns}$.

We calculate avalanche rates and average velocities as a function of electric and magnetic fields and the angle between them and use the following dimensionless substitutes for these parameters:

$$\delta_0 = \frac{E}{E_t}, \quad \eta_0 = \frac{cB}{E_t}, \quad \mu_0 = \cos(\widehat{\mathbf{E}, \mathbf{B}}). \quad (22)$$

3. Runaway Breakdown Results

3.1. Calculated Avalanche Rates

We choose $\mathbf{E} = E_x \hat{\mathbf{x}} + E_z \hat{\mathbf{z}}$ and $\mathbf{B} = B_z \hat{\mathbf{z}}$ and store momentum components p_x, p_y, p_z and coordinates x, y, z for each electron in the set. The calculation is started by introducing a few electrons of energy 1 MeV in the direction opposite to \mathbf{E} . In the absence of a magnetic field the number of electrons grows as shown in Figure 2 for three different values of normalized electric field δ_0 . One can see from Figure 2 that the growth is exponential. Assuming time dependence of $N_r(t)$ to be proportional to e^{Rt} , we can find the avalanche rate R . Figure 3 shows the calculated avalanche rates expressed in a dimensionless form for different δ_0 as a function of normalized magnetic field η_0 for $\mathbf{B} \perp \mathbf{E}$. The data for this plot are given also in Table 1. The statistical error in R is calculated using the fact that the error in the number of particles is $\sqrt{N_r}$.

Calculated rate values R at $\eta_0 = 0$ are ~ 10 times less than those of Roussel-Dupré et al. [1994], which

were used in our previous calculations [Lehtinen et al., 1997], and which were apparently inaccurate [Symbalisty et al., 1997] as discussed in the introduction. With the lower values of R , larger electric fields or longer avalanche distances are required in order to produce a significant number of runaways in the middle atmosphere. Figure 4 shows how particles are distributed in momentum space for different values of η_0 , for $\mathbf{B} \perp \mathbf{E}$. Results indicate a significant $\mathbf{E} \times \mathbf{B}$ drift in addition to the motion in the plane of \mathbf{E} and \mathbf{B} . Figure 5 shows the calculated self-similar electron momentum distributions in the absence of a magnetic field for two different values of δ_0 . The electron momentum distributions are calculated using a total of 2×10^4 Monte Carlo particles, by counting the number of particles in each bin of $\Delta(\ln \mathcal{E}) \approx 0.22$, $\Delta(\cos \theta) = 0.2$. The statistical error estimate for the $\theta = 0$ curve is shown with horizontal dashed lines. In form, the distribution functions resemble those obtained by kinetic calculations [Roussel-Dupré et al., 1994].

3.2. Analytical Analysis of Avalanche Rates

Let us consider the case without a magnetic field, with $\mathbf{B} = 0$. The motion of electrons is then axially symmetric with the axis of symmetry being along $\mathbf{E} = -E\hat{\mathbf{z}}$. An electron whose initial momentum $\mathbf{p}_0 = p_0\hat{\mathbf{z}}$ is opposite to \mathbf{E} , can become a runaway or start an avalanche, or can gradually lose energy in collisions and thermalize. Its “fate” is determined by the rate of frictional energy loss (dynamic friction function) and by the rate of parallel momentum loss (redirection to perpendicular components) due to elastic collisions.

The electronic collisions are a stochastic process; therefore we can only assign a probability for an electron to become a runaway or start a runaway avalanche. Using the Monte Carlo technique, we can estimate this probability by running the simulation many times and approximating the probability with the fraction of runs in which the electron eventually gains energy $\gtrsim 50 mc^2$. In Figure 6, we plot the probability for an electron with given initial momentum vector to become a runaway, calculated in this way. The electric force $-e\mathbf{E}$ on the electron is upward. The probability for an electron to start an avalanche (i.e., create several new electrons) was also calculated and turned out to be almost the same, within statistical error. The white line is a separatrix of the runaway region calculated from a deterministic equation of motion (1) with $\mathbf{\Gamma} = -\hat{\mathbf{p}}F_D$, which neglects stochastic scattering [Gurevich et al., 1992; Roussel-Dupré et al.,

1994]. Above it, in the absence of angular diffusion, electrons are in the runaway region, whereas below it, they are gradually slowed down. We see that, since the motion of the electrons is stochastic, this boundary is in fact diffuse. There is a finite probability for an electron with a small energy (less than the minimum energy given by the white line) to become a runaway, if it by chance experiences less energy losses than average. On the other hand, there is a possibility for electrons with higher energy to lose all of their energy in collisions and thermalize. The boundary of the runaway region, which was calculated using Monte Carlo calculations, lies at a higher value of p than predicted by the deterministic separatrix, due to elastic scattering. This value is estimated analytically as explained below and is represented in Figure 6 by the circle.

We now confirm the results of our Monte Carlo computation by finding the avalanche rates analytically from the Fokker-Planck equation [Roussel-Dupré *et al.*, 1994] for the momentum distribution function $f(\mathbf{p}, t) = f(p, \mu, t)$, where $\mu = \cos \theta$, θ is the angle between the electron momentum and electric force $q\mathbf{E} = -e\mathbf{E}$. This equation can be written in the form:

$$\frac{\partial f}{\partial t} = \frac{1}{p^2} \frac{\partial}{\partial p} \{p^2(F_D - qE\mu)f\} + \frac{\partial}{\partial \mu} \left\{ (1 - \mu^2) \left(-\frac{qE}{p} f + D \frac{\partial f}{\partial \mu} \right) \right\} + S_i(\mathbf{p}) \quad (23)$$

where $q = -e$, F_D is the dynamic friction force, D is the angular diffusion coefficient due to small-angle collisions, S_i is the ionization integral depending on electron distribution f :

$$S_i(\mathbf{p}) = S_i(p, \mu) = \int N_m Z_m v' \frac{d\sigma_{\text{ion}}}{d^3\mathbf{p}}(\mathbf{p}', \mathbf{p}) f(\mathbf{p}') d^3\mathbf{p}'. \quad (24)$$

Note that here primed variable \mathbf{p}' is the momentum of the primary electron and \mathbf{p} of the secondary electron, contrary to the convention of (14) and equations following it. In equation (23), the derivative terms in the right-hand side can be interpreted as follows. The $\partial/\partial p$ describes changes in p without changes in direction, due to dynamic friction and an electric force component $qE \cos \theta$. The $\partial/\partial \mu$ describes changes in the direction of \mathbf{p} , due to an electric force component $qE \sin \theta$, which “bunches” electrons in the forward direction, and the angular diffusion which scatters electrons away from the forward direction. Let us assume that the equilibrium in angles is achieved much faster

than the changes of p take place, due to the relatively high value of D . This condition must be true in particular near the boundary of the runaway region, where p changes relatively slowly. The equation for the angular equilibrium is obtained by equating the $\partial/\partial \mu$ term to zero:

$$\frac{\partial}{\partial \mu} \left\{ (1 - \mu^2) \left(-\frac{qE}{p} f + D \frac{\partial f}{\partial \mu} \right) \right\} = 0,$$

the solution of which is

$$f(p, \mu, t) = C(p, t) \exp \left(\mu \frac{qE}{pD} \right). \quad (25)$$

We now return to equation (23). After substituting a self-similar distribution function such that $\partial f/\partial t = Rf$, and averaging over angles, (23) can be rewritten as

$$Rf_p = \frac{1}{p^2} \frac{\partial}{\partial p} \{p^2[F_D - qEM(p)]f_p\} + S_{ip}(p), \quad (26)$$

where

$$f_p(p, t) = \frac{1}{2} \int_{-1}^1 f(p, \mu, t) d\mu,$$

$$M(p) = \frac{1}{2f_p} \int_{-1}^1 \mu f(p, \mu, t) d\mu,$$

and

$$S_{ip}(p) = \frac{1}{2f_p} \int_{-1}^1 S_i(p, \mu) d\mu.$$

The function $M(p)$, which is just the average value of μ at given p , can be found from equation (25).

The growth rate R can be found from equation (26) using analysis analogous to [Gurevich *et al.*, 1994]. First, note that after we integrate equation (26) over p (with weight $4\pi p^2$), by taking the lower limit at momentum p_s such that $F_D(p_s) = qEM(p_s)$, the $\partial/\partial p$ term disappears, i.e. there is no electron flux through the sphere $p = p_s$. We should thus take p_s to be the boundary of the runaway region. The equality $F_D = qEM$ also intuitively means that the friction is balanced by the electric force component $qE \cos \theta$ parallel to \mathbf{p} . The value of p_s as calculated for the case of Figure 6 is represented in Figure 6 by a circle.

Following Gurevich *et al.* [1994], we assume that in the ionization integral S_{ip} the electrons are described by a monoenergetic beam:

$$f_p(p') = \frac{N}{4\pi p^2} \delta(p' - p_0),$$

which reduces the ionization integral to

$$S_{ip} = \frac{1}{4\pi p^2} N N_m Z_m v_0 \frac{d\sigma_{\text{ion}}}{dp}(p_0, p).$$

We now integrate equation (26) from p_s to ∞ (with weight $4\pi p^2$) to obtain:

$$R \int_{p_s}^{\infty} f_p 4\pi p^2 dp = N N_m Z_m v_0 \int_{p_s}^{\infty} \frac{d\sigma_{\text{ion}}}{dp}(p_0, p) dp$$

Equating the total number of runaway electrons in the left-hand side to N , we find, after changing the integration variable to energy \mathcal{E} :

$$R = N_m Z_m v_0 \int_{\mathcal{E}_s}^{\infty} \frac{d\sigma_{\text{ion}}}{d\mathcal{E}}(\mathcal{E}_0, \mathcal{E}) d\mathcal{E},$$

where \mathcal{E}_s is the critical runaway energy, corresponding to p_s , and \mathcal{E}_0 (corresponding to p_0) is the typical energy of electrons in the beam. This expression is similar to that obtained by *Gurevich et al.* [1992], however, there is a significant conceptual difference. *Gurevich et al.* [1992] neglect angular diffusion and use instead of \mathcal{E}_s the minimum energy of an electron moving initially perpendicular to the electric field necessary for it to run away. The cross section of ionization into interval $d\mathcal{E}$ (for small \mathcal{E}) is

$$\frac{d\sigma_{\text{ion}}}{d\mathcal{E}}(\mathcal{E}_0, \mathcal{E}) \approx \frac{2\pi r_0^2 m c^4}{v_0^2 \mathcal{E}^2}$$

New electrons can be produced by a beam of energy \mathcal{E}_0 only in the interval $\mathcal{E}_s < \mathcal{E} < \mathcal{E}_0/2$, therefore $(d\sigma_{\text{ion}}/d\mathcal{E})(\mathcal{E}_0, \mathcal{E}) \equiv 0$ outside of this interval. We find

$$\begin{aligned} R &= \frac{\partial N}{\partial t} \\ &= \frac{2\pi N_m Z_m r_0^2 m c^4}{v_0} \int_{\mathcal{E}_s}^{\mathcal{E}_0/2} \frac{d\mathcal{E}}{\mathcal{E}^2} \\ &= \frac{2\pi N_m Z_m r_0^2 m c^4}{v_0} \left(\frac{1}{\mathcal{E}_s} - \frac{2}{\mathcal{E}_0} \right), \end{aligned}$$

or in dimensionless units

$$R_d = R\tau = \frac{1}{\beta_0} \left(\frac{1}{\gamma_s - 1} - \frac{2}{\gamma_0 - 1} \right)$$

Using a more exact expression for the ionization cross section as given by (14), we find

$$\begin{aligned} R_d &= \frac{1}{\beta_0} \left(\frac{1}{\gamma_s - 1} - \frac{1}{\gamma_0 - \gamma_s} + \right. \\ &\quad \left. \frac{\gamma_0 - 2\gamma_s + 1}{2\gamma_0^2} - \frac{2\gamma_0 - 1}{\gamma_0^2(\gamma_0 - 1)} \ln \left[\frac{\gamma_0 - \gamma_s}{\gamma_s - 1} \right] \right) \end{aligned} \quad (27)$$

For $\gamma_0 \rightarrow \infty$, we have

$$R_d = 1/(\gamma_s - 1). \quad (28)$$

The justification of the choice of a monoenergetic distribution function and $\gamma_0 \rightarrow \infty$ is essentially simplicity of treatment and our estimates indicate that these choices lead to negligible error. The correct rate is obtained by a convolution of (27) with the electron distribution function. Using self-similar distributions obtained in our Monte Carlo model, we find that this convolution is different from the expression given by simple formula (28) by a factor ranging from ~ 0.8 at $\mathcal{E}_s = 500$ keV to ~ 1.01 at $\mathcal{E}_s = 10$ keV.

Analytical result (28) agrees well with our Monte Carlo calculations, as illustrated in Figure 7. The rate comparisons and values of \mathcal{E}_s are also presented in Table 2. If we “turn off” elastic angular scattering by substituting $M(p) \equiv 1$, the avalanche rates are larger by a factor of ~ 4 , as shown in Figure 7.

3.3. Discussion

The avalanche rates calculated by different authors, which are presented in Figure 7, are apparently quite different. While the results of [*Roussel-Dupré et al.*, 1994], as was shown by [*Symbalisty et al.* 1997, 1998], were overestimated due to numerical error, the rates calculated with a two dimensional kinetic model of [*Symbalisty et al.* 1998] still appear to be greater than both the predictions of our Monte Carlo model and our analytical computations by a factor ranging from ~ 1.5 at $\delta_0 = 2$ to ~ 3.5 at $\delta_0 = 10$. The source of this discrepancy probably lies in the formulation of the ionization process. Assuming that the scattering occurs only at a right angle [*Roussel-Dupré et al.*, 1994], the differential cross section for creation of electron with momentum \mathbf{p} and energy \mathcal{E} by an electron with momentum \mathbf{p}' and energy \mathcal{E}' can be written as

$$\frac{\partial \sigma_{\text{ion}}}{\partial \mathcal{E} \partial \Omega}(\mathcal{E}', \mathcal{E}, \xi) = \frac{d\sigma_{\text{ion}}}{d\mathcal{E}}(\mathcal{E}, \mathcal{E}') \frac{\delta(\cos \xi)}{2\pi},$$

where $d\Omega$ is the element of solid angle, ξ is the angle between \mathbf{p} and \mathbf{p}' . We can write

$$\cos \xi = \cos \theta' \cos \theta + \sin \theta' \sin \theta \cos(\phi' - \phi),$$

where (θ', ϕ') and (θ, ϕ) are the directions of incident and produced electrons, respectively.

Neglecting the ionization energy, the ionization integral (24) can be transformed into the form [*Roussel-Dupré et al.*, 1994]:

$$S_i(\mathbf{p}) = N_m Z_m v \int d\Omega' \int_{2\mathcal{E}}^{\infty} \frac{\partial \sigma_{\text{ion}}}{\partial \mathcal{E} \partial \Omega}(\mathcal{E}', \mathcal{E}, \xi) f(\mathbf{p}') \frac{p'^2}{p^2} d\mathcal{E}'.$$

Integrating over ϕ' using the properties of the Dirac δ function, we find

$$S_i(\mathbf{p}) = N_m Z_m v \cdot \int_{-1}^1 d\mu' \int_{2\mathcal{E}}^{\infty} G_0(\mu', \mu) \frac{d\sigma_{\text{ion}}}{d\mathcal{E}}(\mathcal{E}, \mathcal{E}') f(\mathbf{p}') \frac{p'^2}{p^2} d\mathcal{E}',$$

where $\mu' = \cos \theta'$, $\mu = \cos \theta$, and

$$G_0(\mu', \mu) = \int_0^{2\pi} \frac{\delta(\cos \xi)}{2\pi} d\phi' = \frac{\Theta(1 - \mu'^2 - \mu^2)}{\pi \sqrt{1 - \mu'^2 - \mu^2}},$$

and $\Theta(x)$ is the Heaviside step function. Instead of the above more complete expression, *Symbalisty et al.* [1998] have the following ionization integral:

$$S_i(\mathbf{p}) = N_m Z_m v \cdot \int_{2\mathcal{E}}^{\infty} \frac{d\sigma_{\text{ion}}}{d\mathcal{E}}(\mathcal{E}, \mathcal{E}') \frac{1}{2} [f(p', \mu'_+) + f(p', \mu'_-)] \frac{p'^2}{p^2} d\mathcal{E}',$$

where $\mu'_{\pm} = \pm \sin \theta = \pm \sqrt{1 - \mu^2}$. This corresponds to a substitution $G_0(\mu', \mu) \rightarrow G_1(\mu', \mu)$, where

$$G_1(\mu', \mu) = \frac{1}{2} [\delta(\mu' - \sqrt{1 - \mu^2}) + \delta(\mu' + \sqrt{1 - \mu^2})].$$

Physically, the usage of G_1 instead of G_0 means that only scattering in the plane of \mathbf{E} is allowed, i.e., \mathbf{p} , \mathbf{p}' , \mathbf{E} lie in the same plane. To see the numerical difference in the determination of the avalanche growth rate R calculated using G_0 and G_1 , let us take a distribution with a spread angle θ_b in the beam:

$$f(\mathbf{p}') = \frac{F(p')}{2\pi p'^2} \delta(\mu' - \mu_b),$$

where $\mu_b = \cos \theta_b > 0$. We then have

$$S_i(\mathbf{p}) = G_{0,1}(\mu_b, \mu) N_m Z_m v \int_{2\mathcal{E}}^{\infty} \frac{d\sigma_{\text{ion}}}{d\mathcal{E}}(\mathcal{E}, \mathcal{E}') \frac{F(p')}{2\pi p'^2} d\mathcal{E}'.$$

The rate of change of the total number of particles is thus given by

$$\left(\frac{\partial N}{\partial t} \right)_{\text{ion}} = \int S_i(\mathbf{p}) d^3\mathbf{p} \propto \int_{-1}^1 G_{0,1}(\mu_b, \mu) d\mu.$$

Therefore the rate R_{G_1} calculated using [Roussel-Dupré et al., 1994; Symbalisty et al., 1998] formulation of the ionization integral is greater than R_{G_0} by a factor of

$$\frac{R_{G_1}}{R_{G_0}} = \frac{\int_{-1}^1 G_1(\mu_b, \mu) d\mu}{\int_{-1}^1 G_0(\mu_b, \mu) d\mu} = \frac{\mu_b}{\sqrt{1 - \mu_b^2}} = \cot \theta_b,$$

As the beam gets narrower at higher applied electric fields $\delta_0 = E/E_t$, the factor $\cot \theta_b$ grows, and we have a growing discrepancy between two models.

In view of the key importance of the avalanche rate in the overall development of the runaway electron beam, it is important that the more accurate rates R_{G_0} are used in any qualitative models of this highly nonlinear process.

3.4. Direction and Velocity of Avalanche

Of practical interest is the case when the breakdown does not start uniformly everywhere in space, but instead starts at some localized point and propagates in space. Such case of non-uniform breakdown was previously studied analytically [Gurevich et al., 1994]. Here we instead use the Monte Carlo technique, since it traces the coordinates x , y , z of each particle. To calculate the e -folding distance, in addition to the temporal avalanche growth rate, we should also know the mean velocity of the beam. In previous works [Gurevich et al., 1996; Lehtinen et al., 1997], the mean beam velocity was calculated on the basis of the deterministic equation of motion of an “average electron,” neglecting stochastic scattering, an assumption which leads to inaccurate results. With our Monte Carlo method, the beam velocity \mathbf{v}_r is accurately determined by sampling average coordinates of electrons that move away from the starting point.

4. Relativistic Electron Runaway in the Middle Atmosphere

We now apply the Monte Carlo method to construct a new model of relativistic electron runaway in the middle atmosphere driven by the quasi-electrostatic thundercloud fields [Pasko et al., 1997]. This new model is similar to the cylindrically symmetric model used in our previous work [Lehtinen et al., 1996] but is specifically designed for a Cartesian coordinate system, with a translational symmetry along a horizontal direction, representing the simplest model of the runaway process with which we can account for non-vertical geomagnetic field. In such a model the charge distribution has to be linear, which can physically represent a thundercloud charge distribution with transverse extent. We describe this model briefly below, by pointing out differences between it and our previous model.

4.1. Model Description

The 2-D model presented uses Cartesian coordinates and is translationally symmetric in the horizontal y direction. The geomagnetic field is $\mathbf{B} = B \cos \alpha \hat{\mathbf{z}} + B \sin \alpha \hat{\mathbf{x}}$, $B = 5 \times 10^{-5}$ T, $\alpha = 30^\circ$, where z is a vertical axis. The initial thundercloud charge consists of two infinitely long charges of linear density $\pm\lambda$ at altitudes of 10 km and 5 km, respectively. The separated dipole charges are assumed to be established over a relatively long time (> 100 s). The induced static charge distribution is calculated in the same manner as described in [Lehtinen *et al.*, 1997]. Subsequently, the positive part of the dipole charge is discharged to ground in 1 ms. We use an exponential ambient ion conductivity profile, as in previous work [Pasko *et al.*, 1997; Lehtinen *et al.*, 1997]. This conductivity profile does not include the effect of cloud aerosols. For computational simplicity, we do not account for the change of conductivity associated with heating of thermal electrons by the electric field. This effect would lead to conventional breakdown and development of streamer channels, requiring grid size in our model to be smaller than the streamer size, which is $\lesssim 10$ m at 70 km altitude [Pasko *et al.*, 1998].

The dynamics of the charge distribution is calculated in a manner similar to [Lehtinen *et al.*, 1997]. We take advantage of the relatively slow variation of the electric field and describe it using a time-varying potential (i.e., quasi-electrostatic approximation).

The runaway electron density N_r is calculated using the fluid equation [Lehtinen *et al.*, 1997], with the source S_0 of MeV electrons provided by cosmic rays:

$$\frac{\partial N_r}{\partial t} + \nabla \cdot (\mathbf{v}_r N_r) = R N_r + S_0(z). \quad (29)$$

The local avalanche rate R and velocity \mathbf{v}_r are functions of dimensionless parameters δ_0 , η_0 , μ_0 defined in (22), and are interpolated from values calculated as discussed in section 3 and stored in a lookup table of δ_0 , η_0 , μ_0 . For δ_0 less than a certain value, there is no avalanche. In these cases, the value of $R \leq 0$ is calculated by extrapolation from the calculated $R > 0$ at higher values of δ_0 . These R behave roughly in the same way as those obtained using physical reasoning outlined by Lehtinen *et al.* [1997]. The crudeness of this approximation can be justified by the fact that in the middle atmosphere the regions where the avalanche is quenched do not have many energetic electrons and therefore do not play any role in the development of the avalanche.

The optical emissions are produced as a result of excitation of neutral species through impacts by thermal electrons, driven by the electric field [Pasko *et al.*, 1997], and suprathermal electrons ($\gtrsim 10$ eV), created in the runaway avalanche [Bell *et al.*, 1995]. The optical emission intensities are calculated in the same manner as described by Lehtinen *et al.* [1997].

Gamma ray production is also calculated as by Lehtinen *et al.* [1997], except that we use the new electron distribution in momentum space, obtained by Monte Carlo simulation for parameters δ_0 , η_0 , and μ_0 corresponding to the point at which the volume emission rate proportional to $N_m N_r$ has a maximum, which occurs at ~ 65 km altitude. The emission diagrams of each particle in the set are then summed. We use the Heitler total bremsstrahlung cross section [Heitler, 1954, p. 245]. For N_2 and O_2 and for electron initial and final kinetic energies ~ 1 MeV we can use the Born approximation [Heitler, 1954]. The angular dependence is taken from [Jackson, 1975, p. 705]. Because the atmosphere is optically thin ($\tau \lesssim 0.01$) at the altitude of maximum volume emission rate, we do not take Compton scattering or the photoelectric attenuation effect into account in our calculations of the gamma ray flux at the satellite altitudes.

4.2. Results

Results for a model middle atmosphere are presented in Figures 8 and 9 for a discharge which removes a linear charge density $\lambda = 12$ C/km. For calculations of values integrated over the total volume including the axis of symmetry we assume the size of the region over which charge is removed to be $L = 100$ km, so that the total charge removed in the discharge is $Q = \lambda L = 1200$ C. The cloud length of 100 km is the minimum possible length for which the assumption of approximate translational symmetry is still valid, because it is of the order of nonsymmetric dimensions of the system. The discharge can have a significant effect on the electric field at altitudes where the typical time of field relaxation ϵ_0/σ is greater than the time of discharge. To get the maximum observed currents of ~ 200 kA, the charge 1200 C has to be removed in time in ~ 6 ms, which in our model would have the same effect as instantaneous removal at altitudes below 80 km. The geomagnetic field dip angle for these results is 60° , which corresponds to midlatitudes, where sprites are usually observed. We can use the fluid model of the runaway avalanche when the spatial diffusion of runaway electrons due to different effect of magnetic field on elec-

trons with different energy is not too large. Such is the case for a 60° dip angle, when the geomagnetic field \mathbf{B} is sufficiently close to the vertical. The spatial diffusion of electrons becomes important when \mathbf{B} is close to a horizontal, i.e., at the geomagnetic equator. The orbit of the CGRO satellite on which the gamma ray flashes were measured is confined to $\pm 20^\circ$ geographic latitudes, so that some terrestrial gamma ray flashes may have originated at the geomagnetic equator, where the fluid model is insufficient for their accurate description.

Figure 8a shows the trajectories of runaway electrons calculated on the basis of our Monte Carlo model and the fluid model. We see that electrons move along \mathbf{E} at lower altitudes and along \mathbf{B} at higher altitudes. The altitude at which the regime of motion changes is around 35 km, which is the argument that elastic collisions play a more important role than inelastic ones [Roussel-Dupré and Gurevich, 1996; Taranenko and Roussel-Dupré, 1997]. There is also a drift velocity component perpendicular to the plane of the picture at higher altitudes, where the influence of magnetic field on electron motion is important.

The regions of runaway and conventional air breakdown, which occurs at $\delta_0 \gtrsim 10$ are shown in Figure 8c. Figure 8d shows the two dimensional structure of the runaway beam. The basic difference with our previous work [Lehtinen et al., 1997] is that the runaway density grows slower, since the avalanche rates are smaller by a factor of ~ 10 than those used in [Lehtinen et al., 1997].

Figure 8e shows total optical emissions in the 1st positive band system of N_2 . The intensity in Rayleighs is obtained by integrating the emission rate along the line of sight, which is taken parallel to the linearly extended charge distribution and is thus $L = 100$ km long. Figure 8f shows the relatively weak optical emissions produced by the electrons in the runaway beam, indicating that the emission rate is dominated by the conventional breakdown. Note that Figure 8e shows emissions before conventional breakdown, because our model does not take into account the change of conductivity associated with heating. Therefore, averaged over the frame rate (~ 17 ms) the total emission intensities will be smaller. Nevertheless, comparison of Figures 8e and 8f illustrates that the contribution to the optical intensities of the runaway process is negligible, unlike our previous result reported by Lehtinen et al. [1997].

Figure 9 demonstrates bremsstrahlung gamma ray emissions. A sample of observational data is in Fig-

ure 9a. Figure 9b shows the calculated emissions at 500 km altitude of the observing satellite. The angular distribution of the emission is forward directed for relativistic electrons, which produces the “spot.” As seen from Figure 9b, the angular distribution of emitted gamma rays has a width of $\sim 15^\circ$. Figure 9c is a cartoon demonstrating the production of this spot. The prediction is that for midlatitudes the gamma ray emissions are aligned with the geomagnetic field. Unfortunately, the direction of origin of the terrestrial gamma ray flash requires a special analysis of BATSE data and is not in the public domain, so we cannot draw a conclusion about a correlation between it and the geomagnetic field. The calculated gamma ray flux is of the same order of magnitude as the CGRO observation [Fishman et al., 1994].

The experimental spectra of terrestrial gamma rays [Nemiroff et al., 1997] have been shown to be close to that expected from the bremsstrahlung process. The model described in this work predicts analogous spectra since they are not modified by Compton scattering in the atmosphere.

5. Summary and Conclusions

A Monte Carlo model is used to accurately calculate uniform runaway electron avalanche rates in constant electric and magnetic fields and to determine conditions for an electron to start an avalanche. Our results indicate that several previous calculations of avalanche rates have overestimated them due to numerical problems or simplifying assumptions. The new method is applied to a model of runaway breakdown due to a positive return stroke from a laterally extensive thundercloud using a Cartesian (translationally symmetric) model and a lookup table of calculated avalanche velocities and rates. We conclude that the geomagnetic field must be accounted for in describing the motion of runaway electrons at midlatitudes, where most sprites have been observed. The magnetic field significantly deflects the runaway beam from the vertical, so that the frequently observed vertical columnar structure of sprite is an indication that the observed luminosity is not produced by the runaway electrons as has been previously suggested [Taranenko and Roussel-Dupré, 1996]. At latitudes close to the geomagnetic equatorial region, where terrestrial gamma ray flashes have been detected, the gamma ray beam, which is parallel to the electron beam, is deflected from the vertical due to the geomagnetic field. At the geomagnetic equator, the hor-

horizontal geomagnetic field is perpendicular to the vertical thunderstorm electric field and can prevent the development of relativistic electron avalanche at altitudes $\gtrsim 40$ km.

The optical emissions associated with relativistic electrons are found to be not of significant intensity compared to emissions caused by conventional type of ionization breakdown. For sufficiently large discharge values, the gamma ray fluxes, which are produced by bremsstrahlung from the runaway electron beam, are found to be consistent with experimental data [Fishman *et al.*, 1994; Nemiroff *et al.*, 1997]. The gamma ray spectrum is consistent with a bremsstrahlung spectrum.

In general, the effect of runaway electrons in the upper atmosphere is smaller than in [Lehtinen *et al.*, 1997], due to lower calculated avalanche rates than in [Roussel-Dupré *et al.*, 1994], although the electric field configuration is determined by the same conductivity profile. Other works [e.g., Yukhimuk *et al.*, 1999] use new avalanche rates calculated by Symbalisty *et al.* [1998], which are still larger than those obtained in our Monte Carlo model, as discussed in section 3.3. Also, many works use an electric field model which assumes no conductivity below 20 km [e.g., Roussel-Dupré *et al.*, 1998; Yukhimuk *et al.*, 1999]. The electric field in these models has higher values at altitudes at which the runaway electron avalanche occurs. All these factors lead to lower runaway electron effects in our model than those obtained e.g., by Yukhimuk *et al.* [1999].

Acknowledgments. This work was supported by NASA under grant NAGW4738 to Stanford University.

Janet G. Luhmann thanks Robert Nemiroff and another referee for their assistance in evaluating this paper.

References

- Babich, L. P., and I. M. Kutsyk, Numerical simulation of a nanosecond discharge in helium at atmospheric pressure, developing in the regime of runaway of electrons, *High Temperature*, *33*, 190, 1995.
- Bell, T. F., V. P. Pasko, and U. S. Inan, Runaway electrons as a source of red sprites in the mesosphere, *Geophys. Res. Lett.*, *22*, 2127, 1995.
- Bethe, H. A., and J. Ashkin, *Experimental Nuclear Physics*, edited by E. Segrè, vol. 1, John Wiley, New York, 1953.
- Bulanov, S. V., M. Lontano, P. V. Sasorov, Ionization rate in the presence of runaway electrons, *Phys. Plasmas*, *4*, 931, 1997.
- Fishman, G. J., P. N. Bhat, R. Malozzi, J. M. Horack, T. Koshut, C. Kouveliotou, G. N. Pendleton, C. A. Meegan, R. B. Wilson, W. S. Paciesas, S. J. Goodman, and H. J. Christian, Discovery of intense gamma-ray flashes of atmospheric origin, *Science*, *264*, 1313, 1994.
- Gurevich, A. V., G. M. Milikh, and R. A. Roussel-Dupré, Runaway mechanism of air breakdown and preconditioning during a thunderstorm, *Phys. Lett. A*, *165*, 463, 1992.
- Gurevich, A. V., G. M. Milikh, and R. A. Roussel-Dupré, Nonuniform runaway air-breakdown, *Phys. Lett. A*, *187*, 197, 1994.
- Gurevich, A. V., J. A. Valdivia, G. M. Milikh, and K. Papadopoulos, Runaway electrons in the atmosphere in the presence of a magnetic field, *Radio Sci.*, *31*, 1541, 1996.
- Heitler, W., *The Quantum Theory of Radiation*, 3rd ed., Clarendon, Oxford, 1954.
- Inan, U. S., S. C. Reising, G. J. Fishman and J. M. Horack, On the association of terrestrial gamma-ray bursts with lightning and implication for sprites, *Geophys. Res. Lett.*, *23*, 1017, 1996.
- Jackson, J. D., *Classical Electrodynamics*, 2nd ed., John Wiley, New York, 1975.
- Kunhardt, E. E., Y. Tzeng, and J. P. Boeuf, Stochastic development of an electron avalanche, *Phys. Rev. A*, *34*, 440, 1986.
- Lehtinen, N. G., M. Walt, U. S. Inan, T. F. Bell and V. P. Pasko, γ -ray emission produced by a relativistic beam of runaway electrons accelerated by quasi-electrostatic thundercloud fields, *Geophys. Res. Lett.*, *23*, 2645, 1996.
- Lehtinen, N. G., T. F. Bell, V. P. Pasko, and U. S. Inan, A two-dimensional model of runaway electron beams driven by quasi-electrostatic thundercloud fields, *Geophys. Res. Lett.*, *24*, 2639, 1997.
- McCarthy, M. P., and G. K. Parks, On the modulation of X ray fluxes in thunderstorms, *J. Geophys. Res.*, *97*, 5857, 1992.
- Mott, N. F. and H. S. W. Massey, *The Theory of Atomic Collisions*, 3rd ed., Clarendon, Oxford, 1965.
- Nemiroff, R. J., J. T. Bonnell and J. P. Norris, Temporal and spectral characteristics of terrestrial gamma flashes, *J. Geophys. Res.*, *102*, 9659, 1997.
- Papadopoulos, K., G. Milikh, A. Gurevich, A. Drobot, and R. Shanny, Ionization Rates for Atmospheric and Ionospheric Breakdown, *J. Geophys. Res.*, *98*, 17593, 1993.
- Pasko, V. P., U. S. Inan, T. F. Bell and Y. N. Taranenkov, Sprites produced by quasi-electrostatic heating and ionization in the lower atmosphere, *J. Geophys. Res.*, *102*, 4529, 1997.
- Pasko, V. P., U. S. Inan, and T. F. Bell, Spatial structure of sprites, *Geophys. Res. Lett.*, *25*, 2123, 1998.

- Risken, H. *The Fokker-Planck Equation*, 2nd ed., Springer-Verlag, New York, 1989.
- Roussel-Dupré, R. A., A. V. Gurevich, T. Tunnel, and G. M. Milikh, Kinetic theory of runaway breakdown, *Phys. Rev.*, *49*, 2257, 1994.
- Roussel-Dupré, R. A., and A. V. Gurevich, On runaway breakdown and upward propagating discharges, *J. Geophys. Res.*, *101*, 2297, 1996.
- Roussel-Dupré, R., E. Symbalisty, Y. Taranenko, and V. Yukhimuk, Simulations of high-altitude discharges initiated by runaway breakdown, *J. Atmos. Sol. Terr. Phys.*, *60*, 917, 1998.
- Sentman, D. D., E. M. Wescott, D. L. Osborne, D. L. Hampton, and M. J. Heavner, Preliminary results from the Sprites94 campaign: Red sprites, *Geophys. Res. Lett.*, *22*, 1205, 1995.
- Shveigert, V. A., Development of electron avalanche in strong electric fields, *Sov. J. Plasma Phys.*, *14*, 373, 1988.
- Sizykh, S. V., Runaway electron production rate in gaseous discharges, *High Temperature*, *31*, 1, 1993.
- Symbalisty, E., R. Roussel-Dupré, L. P. Babich, I. M. Kut- syk, E. N. Donskoy, and A. Y. Kudryavtsev, Re- evaluation of electron avalanche rates for runaway and upper atmospheric discharge phenomena (abstract), *Eos Trans. AGU*, *78 (46)*, Fall Meet. Suppl., F70, 1997.
- Symbalisty, E. M. D., R. A. Roussel-Dupré, and V. A. Yukhimuk, Finite volume solution of the relativistic Boltzmann equation for electron avalanche rates, *IEEE Trans. Plasma Sci.*, *26*, 1575, 1998.
- Taranenko, Y. and R. Roussel-Dupré, High altitude discharges and gamma-ray flashes: A manifestation of runaway air breakdown, *Geophys. Res. Lett.*, *23*, 571, 1996.
- Taranenko, Y. and R. Roussel-Dupré, Reply, *Geophys. Res. Lett.*, *24*, 2645, 1997.
- Yukhimuk, V., R. Roussel-Dupré, E. M. D. Symbal- istry, and Y. Taranenko, Optical characteristics of Red Sprites produced by runaway air breakdown, *J. Geo- phys. Res.*, *103*, 11473, 1998.
- Yukhimuk, V., R. Roussel-Dupré, and E. M. D. Symbal- istry, On the temporal evolution of red sprites: Runaway theory versus data, *Geophys. Res. Lett.*, *26*, 679, 1999.

N. G. Lehtinen, T. F. Bell, and U. S. Inan, STAR Laboratory, Stanford University, Stanford, CA 94305. (inan@nova.stanford.edu)

Received March 22, 1999; revised June 25, 1999; accepted July 23, 1999.

Figure 1. Dynamic friction function used in our calculations: solid line, full dynamic friction function F_D given in equation (2); dashed line, dynamic friction $F_{D,\text{excl}}$ with excluded ionization given in equation (8).

Figure 2. Growth of the number of particles in the Monte Carlo calculations for different values of δ_0 .

Figure 3. Runaway avalanche growth rate R multiplied by the characteristic time τ defined in equation (21). Shown here is magnetic field dependence for different values of electric field for $\mathbf{E} \perp \mathbf{B}$.

Figure 4. Electrons in momentum space for orthogonal \mathbf{E} and \mathbf{B} , $\delta_0 = 5$: (a) $\eta_0 = 0$ and (b) $\eta_0 = \delta_0$. There is no avalanche at $\eta_0 = 2\delta_0$.

Figure 5. Electron distributions for two different electric field values in the absence of a magnetic field: (a) $\delta_0 = 2$, (b) $\delta_0 = 15$. Also shown is the runaway region of electron energies, calculation of which is discussed later in the text. The horizontal dashed lines show an estimate of a statistical error for $\theta = 0$.

Figure 6. The probability for an electron with a given momentum to become a runaway for $\delta_0 = 5$ and no magnetic field ($\eta_0 = 0$). The direction of \mathbf{E} is downward (electrons accelerate upward). The white line is the boundary of runaway region if the motion of an electron is deterministic. The circle has radius p_s (see text).

Figure 7. Dimensionless runaway avalanche growth rate $R_d = R\tau$ in the absence of magnetic field, as a function of electric field, obtained by different models: (1) analytical expression, (2) Monte Carlo, (3) *Symbalisty et al.* [1998], (4) analytical expression without elastic scattering, and (5) *Roussel-Dupré et al.* [1994].

Figure 8. The runaway electron avalanche in the atmosphere for a charge moment of $\lambda = 12$ C/km at $t = 3$ ms after the start of the discharge. \mathbf{B} lies in the plane of the picture. (a) Velocity field lines, (b) electric field lines, (c) electric field thresholds, (d) runaway electron density, (e) optical emissions in N_2 first positive band system (total), maximum is ~ 6.4 MR. (f) Runaway electron contribution to it, maximum is ~ 8.8 kR.

Figure 9. Terrestrial gamma ray flashes. (a) Sample of BATSE observation, (b) simulated terrestrial gamma ray flashes as seen by BATSE, at $\sim 45^\circ$ northern latitude in the photon energy interval 100–300 keV, and (c) schematics of gamma ray emission.

Table 1. Dimensionless Avalanche Rate $R_d = R\tau$ for Different Parameters $\delta_0 = E/E_t$ and $\eta_0 = cB/E_t$ for $\mathbf{E} \perp \mathbf{B}$

$\eta_0 \setminus \delta_0$	2	5	8	15	30
0	0.955 ± 0.053	4.94 ± 0.27	10.3 ± 0.6	22.5 ± 1.3	60.4 ± 3.6
1	0.867 ± 0.051	5.08 ± 0.29	9.68 ± 0.57	22.9 ± 1.3	56.9 ± 3.4
2	...	4.93 ± 0.29	10.4 ± 0.6	23.2 ± 1.4	59.8 ± 3.5
5	...	4.05 ± 0.24	9.68 ± 0.55	23.2 ± 1.4	59.4 ± 3.7
8	...	0.151 ± 0.009	8.12 ± 0.47	22.7 ± 1.3	57.0 ± 3.3
15	0.741 ± 0.041	20.9 ± 1.2	57.8 ± 3.6
30	9.87 ± 0.58	56.9 ± 3.4

Three dots correspond to a situation without an avalanche. All results are derived for 1500 particles.

Table 2. Monte Carlo Results for $B = 0$, Analytical Estimates

δ_0	2	5	8	10	12	15
R_d , model	0.986 ± 0.014	5.18 ± 0.08	9.92 ± 0.15	13.30 ± 0.19	17.14 ± 0.25	22.66 ± 0.33
\mathcal{E}_s , keV	549	103	54	41	32	24
$R_d = mc^2/\mathcal{E}_s$	0.930	4.92	9.41	12.6	16.0	21.2

Model results are derived for 20,000 particles.

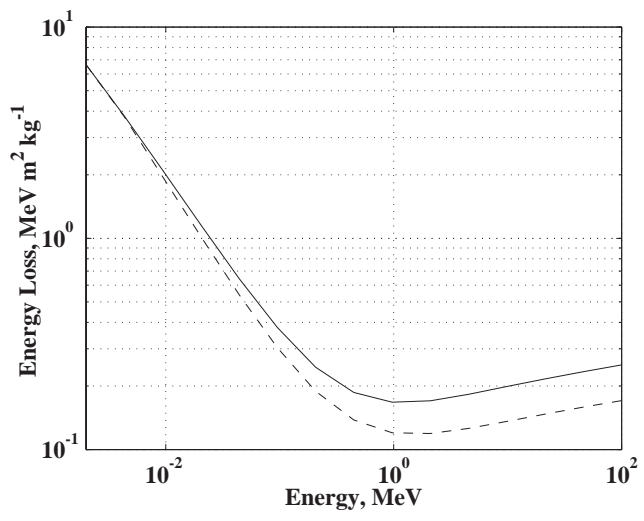


FIGURE 1

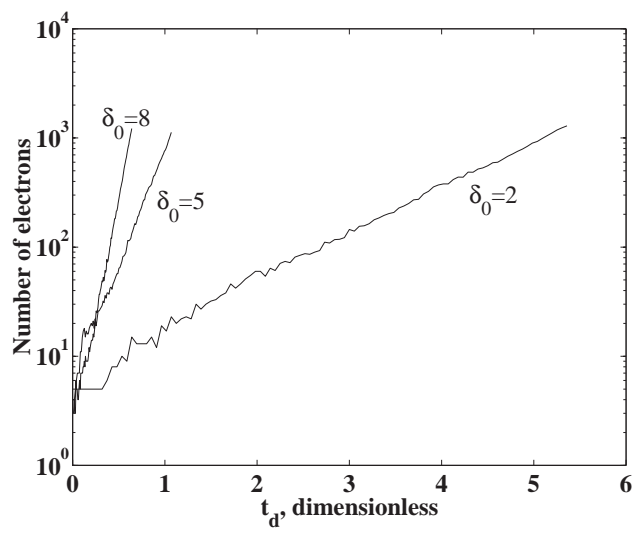


FIGURE 2

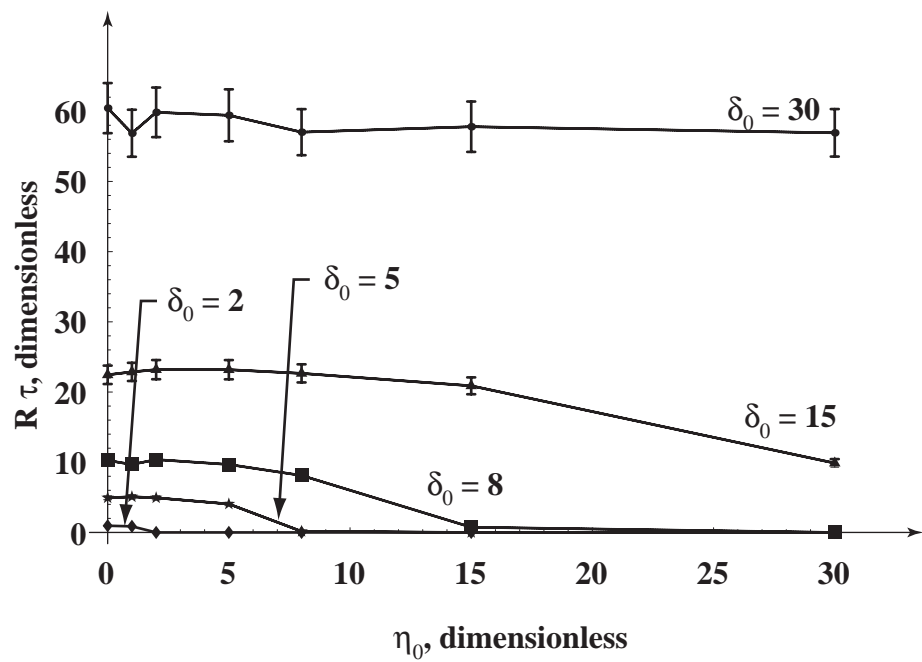


FIGURE 3

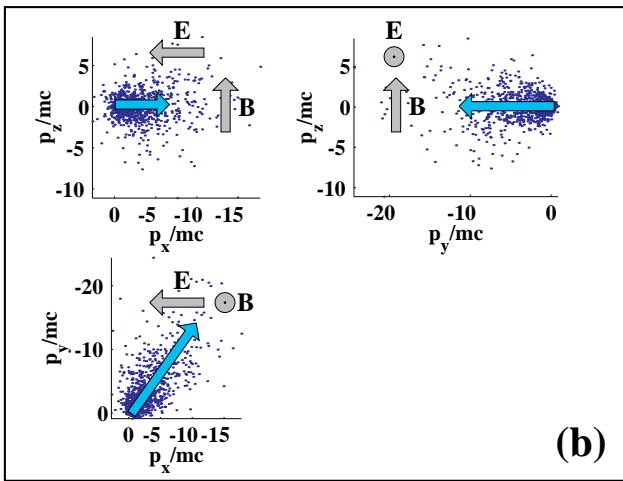
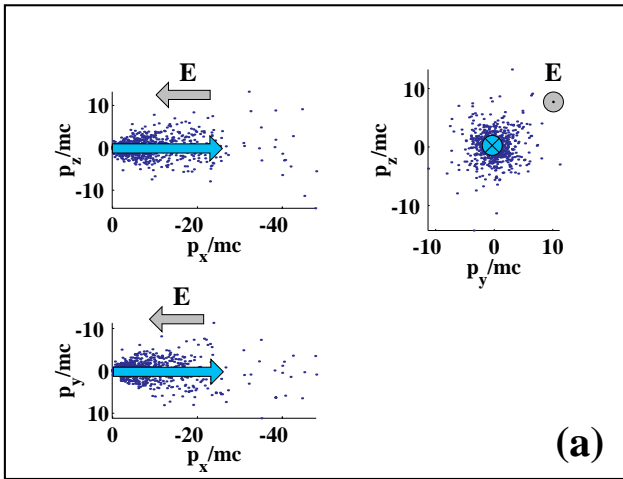


FIGURE 4

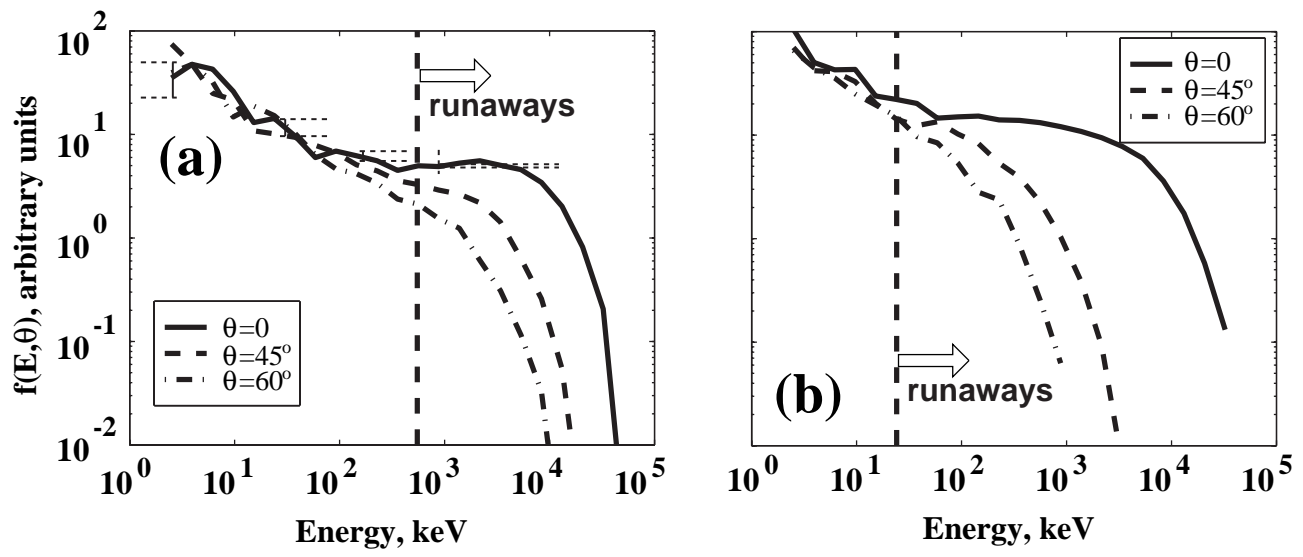


FIGURE 5

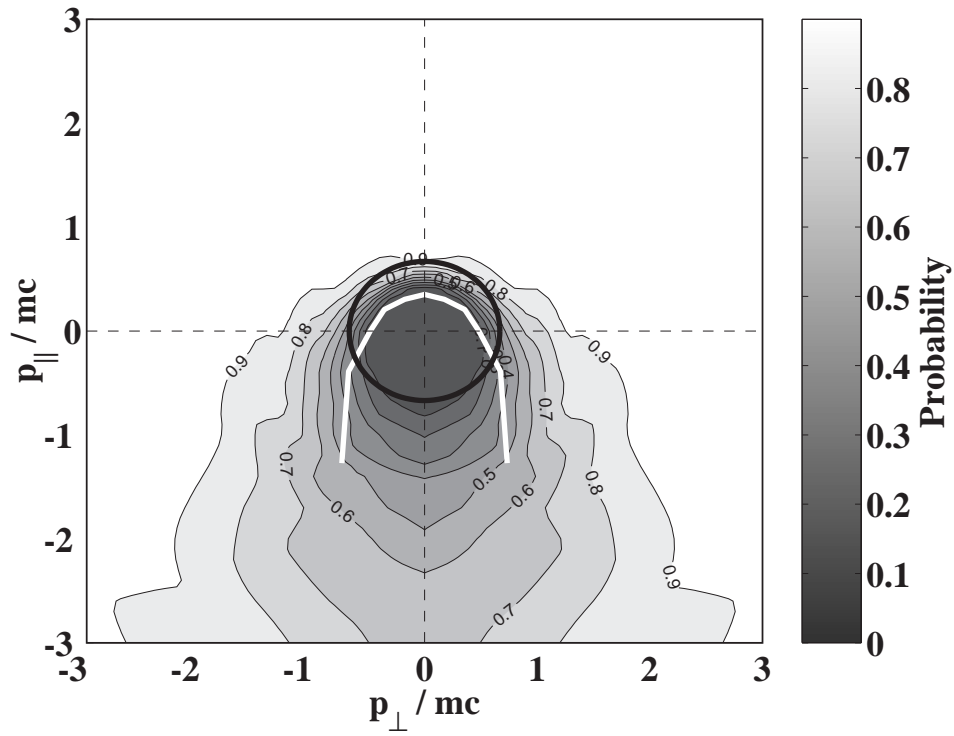


FIGURE 6

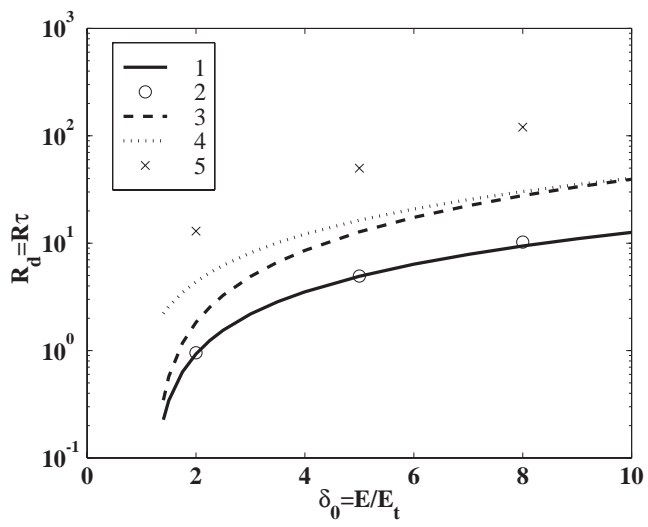


FIGURE 7

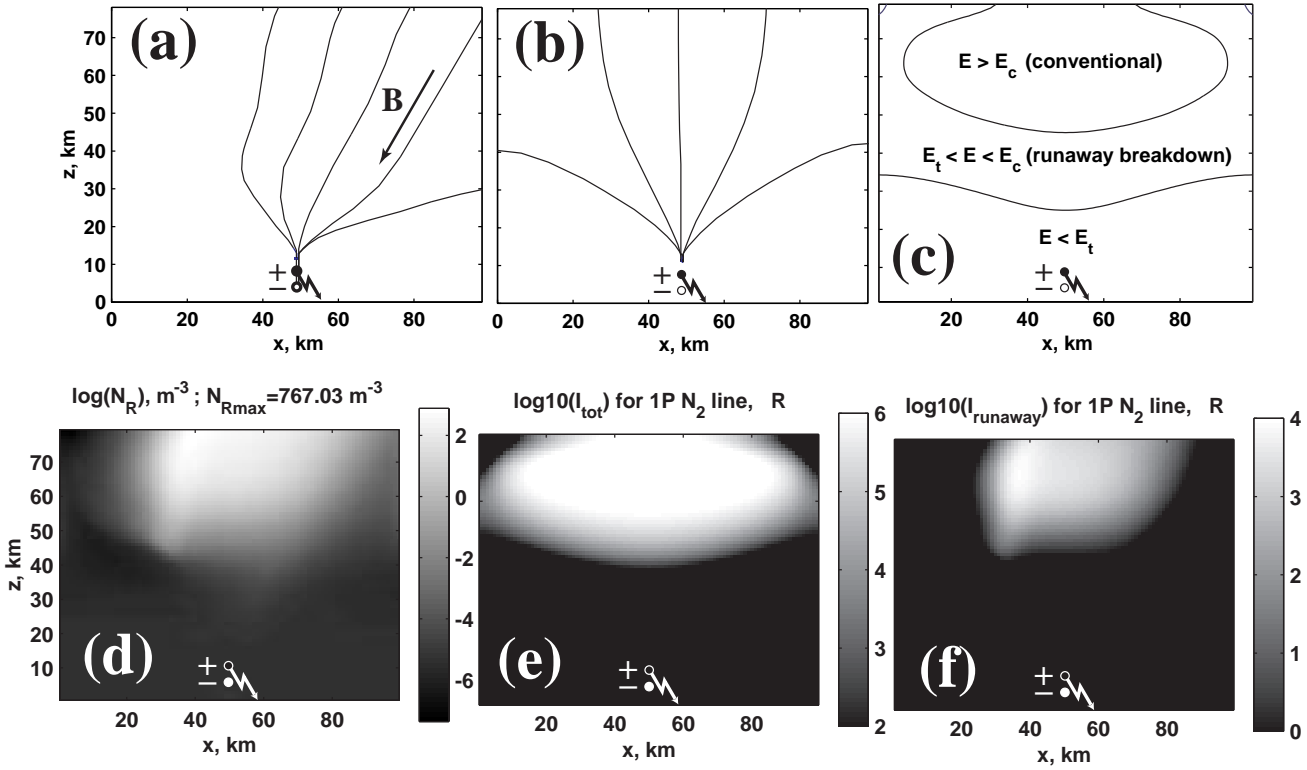


FIGURE 8

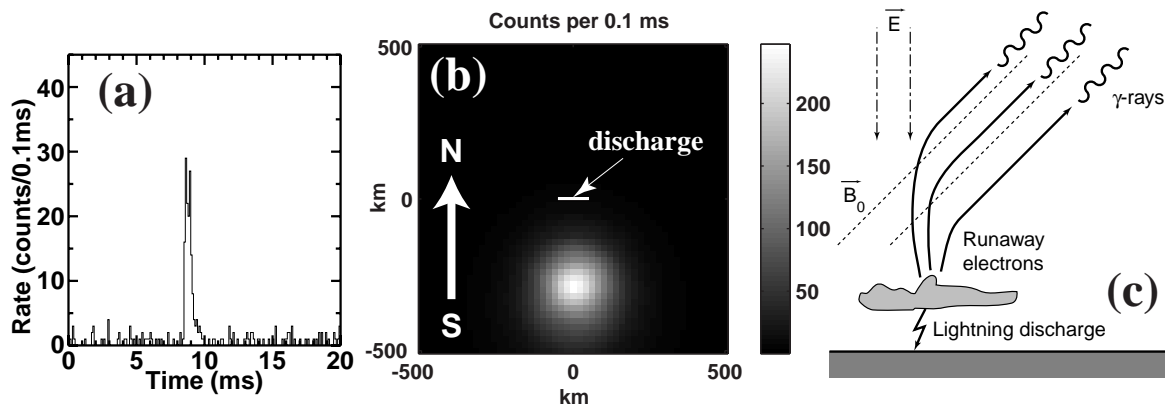


FIGURE 9